Carboxylated, Fe-Filled Multiwalled Carbon Nanotubes as Versatile Catalysts for O_2 Reduction and H_2 Evolution Reactions at Physiological pH

M. Victoria Bracamonte,[a, b] Michele Melchionna,*[a] Antoine Stopin,[c] Angela Giulani,[a] Claudio Tavagnacco,[a] Yann Garcia,[e] Paolo Fornasiero,*[a, d] Davide Bonifazi,[a, c] and Maurizio Prato[a]

Abstract: The development of new electrocatalysts for the oxygen reduction reaction (ORR) and hydrogen evolution reaction (HER) at physiological pH is critical for several fields, including fuel cells and biological applications. Herein, the assembly of an electrode based on carboxyl-functionalised hydrophilic multiwalled carbon nanotubes (MWCNTs) filled with Fe phases and their excellent performance as electrocatalysts for ORR and HER at physiological pH are reported. The encapsulated Fe dramatically enhances the catalytic activity, and the graphitic shells play a double role of efficiently mediating the electron transfer to O_2 and H_2O reactants and providing a cocoon that prevents uncontrolled Fe oxidation or leaching.

Introduction

Current projections identify fuel cells (FCs) as one of the predominant energy devices of the near future, with a crucial role in the development of new technologies for greener energy.[1] This has inspired ever-growing interest in FC technologies on account of their high efficiency and environmental friendliness. The heart of an FC device can simplistically be described in terms of the two half-reactions occurring at the two electrodes: the electrochemical reduction of oxygen ($O_2 + 4e^- + 4H^+ \rightarrow 2H_2O$) at the cathode and oxidation of the fuel at the anode (e.g., with hydrogen as fuel: $2H_2 \rightarrow 4H^+ + 4e^-$). Due to the high bond energy of O_2, the cathodic half-reaction proceeds sluggishly, and this often poses a severe limitation to efficiency.[2] To overcome such a bottleneck, catalysts based on Pt supported on high surface area carbon black are typically employed.[3] Indeed, the E-TEK catalyst (20% Pt/C) is nowadays considered the benchmark catalyst and used as reference in most studies on O_2 reduction. Nevertheless, this type of catalyst is not an economically favourable choice due to the low abundance and geopolitics-dependent availability of Pt and Pd.[4] Moreover, they suffer from low tolerance to most fuel impurities and time-dependent deactivation.[4,5] For this reason, more recent strategies have focused on using less active but more abundant non-precious metals.[4,6]

For the latter half-reaction in an FC device, H_2 is emerging as a highly desirable choice of fuel, especially if it is obtained by the green process of water splitting, and in view of the rapid depletion of fossil fuels. Beside FC applications, production of H_2 is actively pursued due to its crucial role in important industrial processes such as hydrogenation reactions, NH_3 production and oil refining. Particularly intriguing is the production of H_2 through water splitting, which can also be achieved electrochemically with noble metal catalysts such as Pt,[7] Pd,[8] Au and Ir.[9] In this case, too, use of more readily available metals such as Fe has been under investigation.[10]

The above considerations highlight the importance of developing new cost-effective catalysts that efficiently carry out the oxygen reduction reaction (ORR) and hydrogen evolution reaction (HER).[11] Recently, carbon nanotubes (CNTs) have emerged as extraordinary building blocks for the assembly of functional materials.[12] This stems from their unique properties,[13] which led to their use as active scaffolds in a wide range of applications, such as organic photovoltaics,[14] integrated circuits,[15]

[a] *M. V. Bracamonte, Dr. M. Melchionna, A. Giulani, Prof. C. Tavagnacco, Prof. P. Fornasiero, Prof. D. Bonifazi, Prof. M. Prato*
Department of Chemical and Pharmaceutical Sciences and INSTM UdR Trieste, University of Trieste, Via L. Giorgieri 1, 34127 Trieste (Italy)
E-mail: melchionnam@units.it

[b] *M. V. Bracamonte*
Instituto de Física Enrique Gaviola (CONICET) and FaMAF
Universidad Nacional de Córdoba, Medina Allende s/n
X5000HUA Córdoba (Argentina)

[c] *Dr. A. Stopin, Prof. D. Bonifazi*
Namur Research College (NARC) and Department of Chemistry
University of Namur (UNamur), Rue de Bruxelles 61, 5000 Namur (Belgium)

[d] *Prof. P. Fornasiero*
ICCOM-CNR Trieste Research Unit, Trieste (Italy)
E-mail: pfornasiero@units.it

[e] *Dr. Y. Garcia*
Institute of Condensed Matter and Nanosciences, Molecules Solids and Reactivity (IMCN/MOST)
Université Catholique de Louvain, Place L. Pasteur 1
Louvain-la-Neuve, 1348 (Belgium)

biosensors[16] and heterogeneous catalysts.[17] An intriguing possibility is endohedral functionalization of the CNT scaffold.[18] Incorporation of molecular entities or bulk materials in the inner cavity of CNTs is expected to cause confinement effects similar to those found in the pores of zeolites[19] and to have interesting implications in catalysis.[20] Recently, the assembly of a nanocomposite featuring peapod-like multiwalled carbon nanotubes with internal Fe nanoparticles (Fe@MWCNTs) was successfully applied in polymer-electrolyte membrane fuel cells working under acidic conditions.[21] This catalyst was ORR-active and could tolerate the presence of sulfur contaminants owing to the excellent protection provided by the CNT scaffold. On the basis of DFT calculations, the mechanism for O_2 activation was interpreted in terms of an electron transfer from Fe to the CNT with decrease of the local work function on the carbon surface. Moreover, for this system, as well as in other works,[22] doping of the graphitic layer with N atoms has proved to be a promising strategy to improve ORR performance. However, ORR at physiological pH is a relatively unexplored field that is of great interest for engineering various biologically compatible devices[23] including microbial fuel cells.[24] Similarly, the ability to perform HER under mild conditions would be highly desirable, and recently efforts are being made to develop systems that carry out electrocatalytic HER at neutral pH.[25]

Motivated by the need to perform ORR and HER at physiological pH, herein we explore the possibility of assembling specifically designed Fe@MWCNTs for preparing active electrodes for both reactions under physiological conditions. Remarkably, increasing the hydrophilicity and defective nature of the exohedral graphitic layer results in enhancement of the catalytic activity. In contrast to the commonly used oxidation methodologies[26] based on mineral acid treatment causing tip opening, we selected the milder Tour-like radical addition reaction to decorate the graphitic framework with carboxyl groups without compromising the confinement of the Fe phase. Overall, we observe good activities for ORR and decent activities for HER considering the demanding experimental conditions, which prove the versatility of the modified electrode.

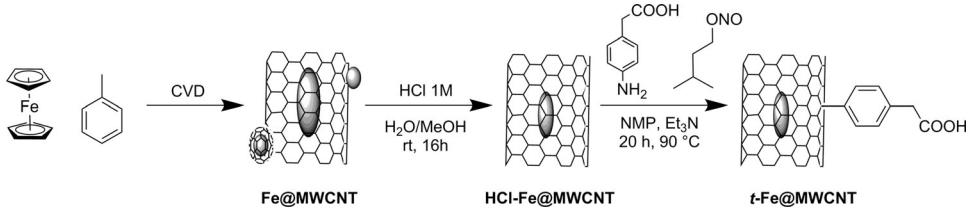

Scheme 1. Synthetic procedure for t-Fe@MWCNT.

Results and Discussion

Synthesis

The Fe@MWCNTs were synthesised by chemical vapour deposition in an oven at 1173 K with ferrocene (Fc, 5 g) as catalyst and Fe source sublimated at 623 K and toluene as an additional carbon source.[28] The crude material was then washed with ethanol and filtered on a hydrophobic polytetrafluoroethylene membrane to remove any externally adsorbed Fc on Fe@MWCNT (Scheme 1). The sample was then washed with 1 M HCl in MeOH/water (3/1 v/v) and filtered to give purified Fe@MWCNTs that contain reduced amounts of spherical aggregates containing Fe. The Fe@MWCNTs were then exohedrally functionalized by a procedure similar to that reported by Tour and Bahr[29] by using *para*-aminophenylacetic acid in the presence of isoamyl nitrite and Et_3N in *N*-methylmorpholine, which led to in situ formation of the corresponding diazononium salt, and thus t-Fe@MWCNT was obtained. Although oxidations with mineral acids are well known to introduce defects and oxygenated carbon species, these protocols are rather aggressive and mainly lead to removal of the tips of the nanotubes.[26,30] In our case, tip opening would be highly detrimental, as internalized Fe might be leached out through the ends of the MWCNTs. The quality of the different Fe@MWCNT materials was then evaluated by macroscopic and microscopic methods.

Macroscopic and Fe-phase characterization

Thermogravimetric analysis (TGA) under N_2 confirmed successful incorporation of the benzylic acid moiety onto the nanotube framework. A weight loss of approximately 3.5% at 452 K was achieved, which is indicative of the presence of organic functional groups. TGA under air caused combustion of all the organic components, including the MWCNTs (weight loss at $\approx$853 K), and in the case of Fe-filled MWCNTs, it gives an estimate of the Fe content. The materials showed a residual inorganic content, attributed mainly to Fe_2O_3, of 31 wt%. Washing with HCl removed the non-encapsulated Fe phases and led to a decrease in Fe content of about 27% (see Supporting Information, Figure S1).

Raman analysis showed the typical fingerprint of the MWCNT framework, (Figure 1) with four main bands: D at about 1351 cm^{-1}, G at about 1588 cm^{-1}, D′ at about 1627 cm^{-1}, and 2D at about 2702 cm^{-1}. Furthermore, combination bands were observed: D + D″ at about 2460 cm^{-1} and D + D′ at about 2958 cm^{-1}. The intensity ratio I_D/I_G is often used as semi-quantitative indication of the degree of covalent functionalization, as an increase of the D band is associated with disruption of the polyaromatic pattern by the addition reaction.[31] For the commercial empty-cavity MWCNTs used here, I_D/I_G was inherently higher ($I_D/I_G = 0.9$), a sign that such materials have a higher number of defect sites than other commercial nanotubes as well as the HCl-Fe@MWCNTs and t-Fe@MWCNT ($I_D/I_G = 0.36 \pm 0.04$).[32] The incorporation of the functional groups was confirmed by FTIR spectroscopy (see Supporting Information, Figure S2).

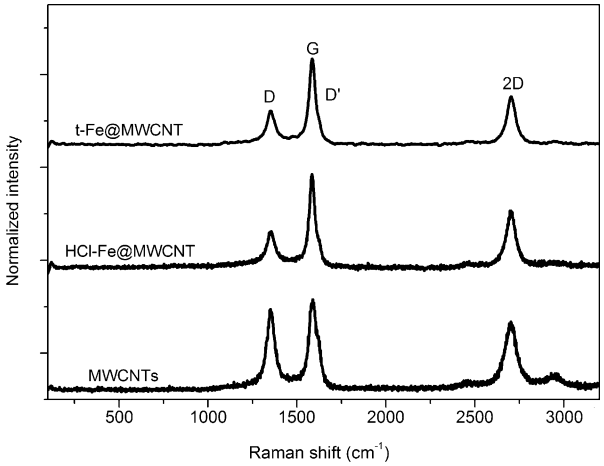

Figure 1. Raman spectra of MWCNTs, HCl-Fe@MWCNTs and t-Fe@MWCNTs.

The Fe phases embedded in the inner cavity were studied by powder (P) XRD and ^{57}Fe Mössbauer spectroscopy. PXRD was carried out on three different Fe-filled MWCNTs and revealed the presence of three Fe phases (α-Fe, γ-Fe and Fe carbide), the relative ratio of which varies with the HCl washing protocol (Figure 2). In as-produced Fe@MWCNT, the presence of α-Fe is clearly evident (peak at 44.6° overlapping with Fe-carbide peak) and decreases after HCl treatment. It is noteworthy that, as expected, the exohedral functionalization does not modify the overall composition of the different Fe phases, as confirmed by the almost identical PXRD spectra for HCl-Fe@MWCNT and t-Fe@MWCNT samples.

^{57}Fe Mössbauer experiments were also performed on Fe@MWCNTs and HCl-Fe@MWCNTs and revealed the presence of α-Fe, γ-Fe and Fe carbide in both samples with different ratios (Figure 3). The respective fractions of each Fe phase in the samples are 25% α-Fe, 33% γ-Fe and 42% Fe carbide for Fe@MWCNTs and 18% α-Fe, 40% γ-Fe and 42% Fe carbide for HCl-Fe@MWCNTs.

Microscopic characterization

TEM analysis of the different samples revealed the presence of MWCNTs of various lengths and diameters with encapsulated Fe in sphere-like shapes, located for the most part at the tip of the MWCNTs, as well as nanorods, located in the middle region of the MWCNTs (Figure 4). Bamboo-like MWCNTs were also observed in the different samples.

Electrochemical characterization

The electrochemical responses of the different materials were studied by cyclic voltammetry between +1.25 and −0.75 V. Figure 5 shows the cyclic voltammograms (CVs) at bare and MWCNTs-, HCl-Fe@MWCNT- and t-Fe@MWCNT-modified glassy carbon electrodes (GCE) in N_2-saturated 0.10 M phosphate buffer solution (pH 7.4) at a scan rate v of 0.03 V s^{-1}. On bare GCE, only low capacitive currents i_{cap} were observed in the studied potential range. In contrast, GCE/MWCNTs showed an

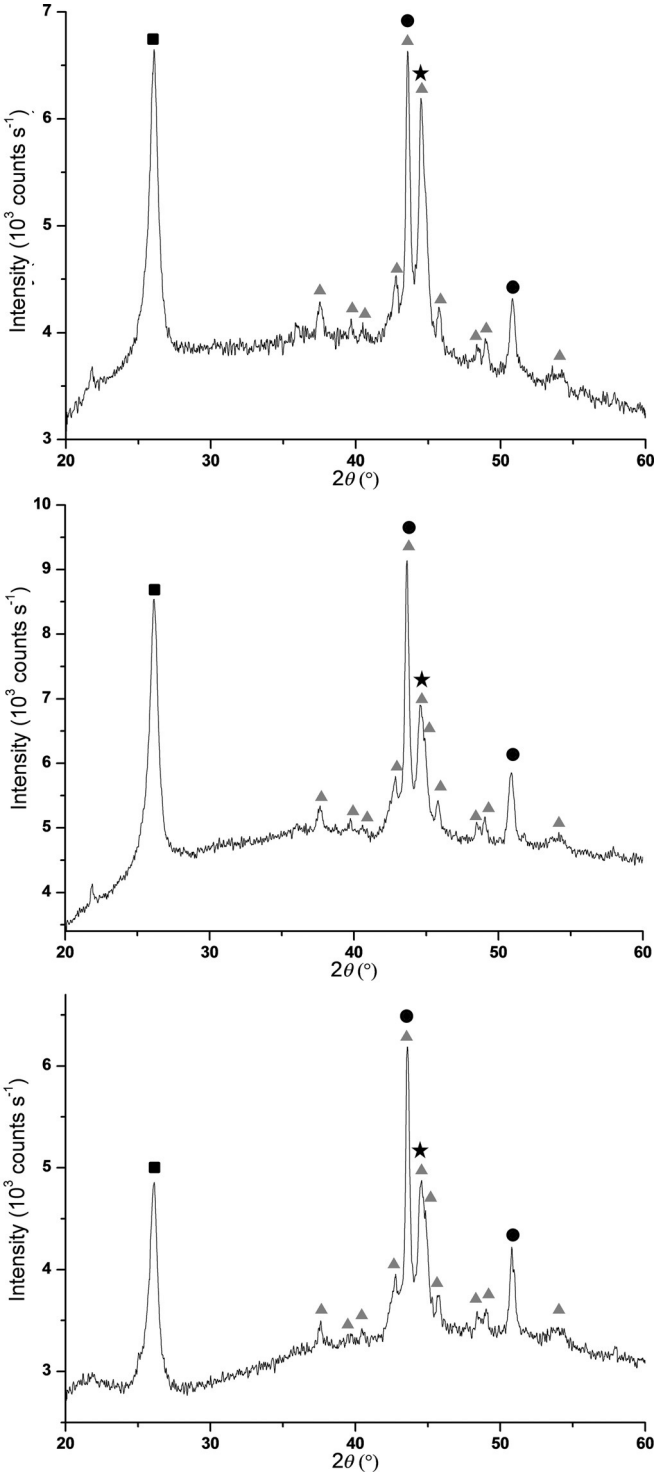

Figure 2. PXRD patterns for Fe@MWCNT (top), HCl-Fe@MWCNT (middle) and t-Fe@MWCNT (bottom). ■ = graphite; ▲ = Fe carbide; star = Fe-α; and ● = Fe-γ.

increase in i_{cap}, correlated with deposition of a modified layer on the surface of the electrodes. The change in i_{cap} observed on the GCE/HCl-Fe@MWCNT electrode indicates variability in the charge or defect density on the modified electrode.[33] Moreover, a broad reduction peak, centred at −0.14 V and at least three oxidation peaks at −0.30, 0.13 and 0.71 V appeared.

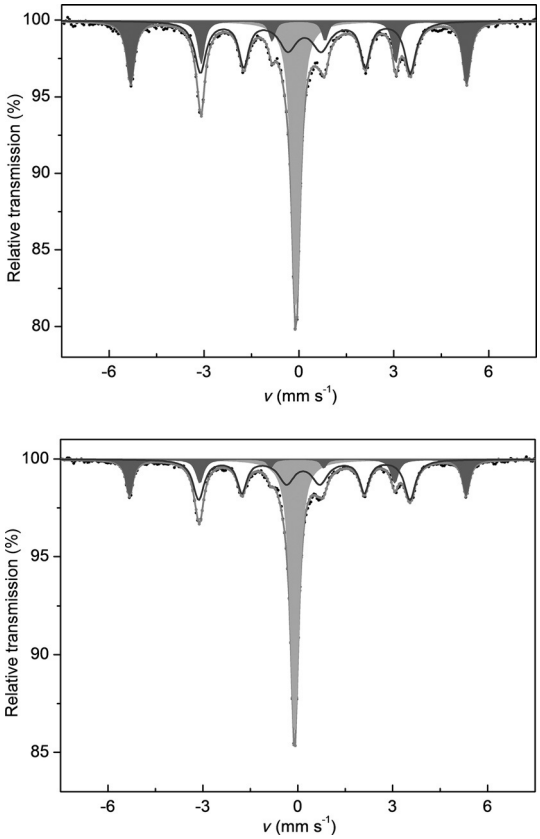

Figure 3. ^{57}Fe Mössbauer spectra of Fe@MWCNTs (top) and HCl-Fe@MWCNTs (bottom) with the expected sextets of α-Fe (grey) and Fe carbide (black) and the expected singlet of γ-Fe (light grey). The grey line is the non-deconvoluted experimental profile.

These signals can be attributed to redox processes occurring between the iron in the nanotubes and the electrode surface.[34] The absence of new signals appears in the CV at GCE/t-Fe@MWCNT revealed that organic functionalization did not introduce any new electrochemical process of the iron-filled

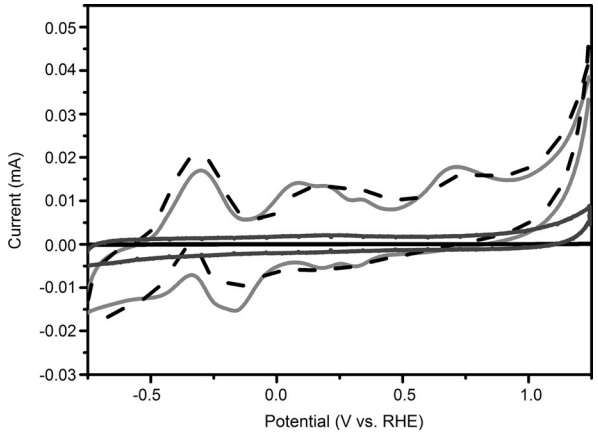

Figure 5. CVs obtained on bare GCE (solid black), GCE/MWCNT (solid dark grey), GCE/Fe@MWCNT (solid light grey) and GCE/t-Fe@MWNCT (dashed) in N_2-saturated 0.10 M phosphate buffer solution (pH 7.40). Scan rate: 0.03 V s^{-1}.

carbon nanotubes. The stability of the modified GCE was also evaluated by measuring 15 repetitive cycles in 0.10 M phosphate buffer solution at $v = 0.03$ V s^{-1} (see Supporting Information, Figure S3), and no substantial leaching of Fe into the solution was observed.

Electrocatalysis

Oxygen reduction reaction

The catalytic activities of the MWCNTS, HCl-Fe@MWCNT and t-Fe@MWCNT for the ORR were screened by performing cyclic voltammetry in the presence of dissolved O_2 in 0.1 M phosphate buffer solution (pH 7.4) at $v = 0.10$ V s^{-1}. We compared the forward CV segments of the unmodified and different modified GCEs in a 2.5 mg L^{-1} O_2-saturated solution (Figure 6, the complete CVs are shown in Supporting Information, Figure S4).

For the GCE, the ORR peak potential E_{peak} was −0.45 V with a peak current i_{peak} of −0.19 mA. Upon loading the GC electrodes with nanotubes, the ORR E_{peak} shifted to −0.35 V for MWNCTs, −0.45 V for HCl-Fe@MWCNTs and −0.25 V for t-Fe@MWCNTs with concomitant increases in i_{peak} (−0.22, −0.51 and −0.99 mA, respectively). These results clearly indicate significant enhancement of the ORR electrocatalytic activity of t-Fe@MWCNTs compared with the pristine MWCNTs and HCl-Fe@MWCNT and highlight the importance of the encapsulated Fe and the organic functionalization for the catalytic activity. The obtained electrochemical

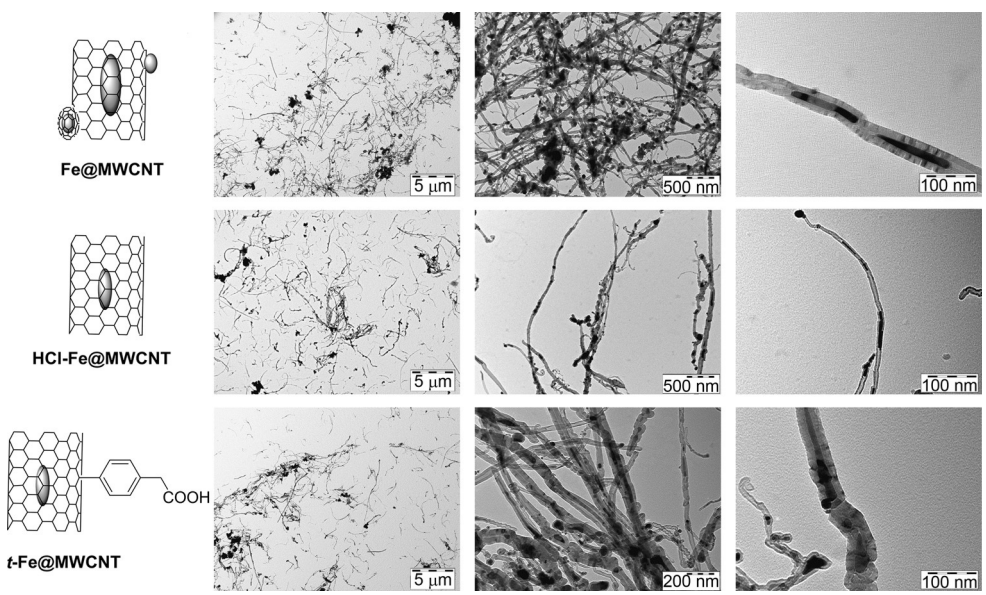

Figure 4. TEM images of Fe@MWCNT, HCl-Fe@MWCNTs and t-Fe@MWCNTs.

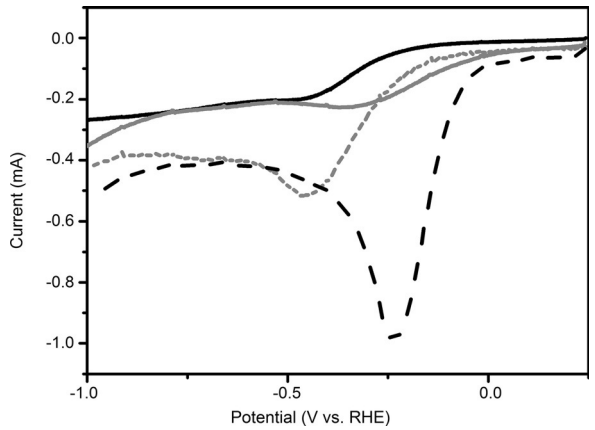

Figure 6. Forward CV segment at bare (solid black), MWCNT- (solid grey), HCl-Fe@MWCNT- (dotted) and t-Fe@MWCNT-modified GCE (dashed) in 2.5 mg L^{-1} O_2 dissolved in phosphate buffer solution. Scan rate: 0.10 V s^{-1}.

response is in agreement with the work of Deng et al.,[21] who described high catalytic activities as the result of a decrease in the local work function on the carbon surface due to electron-transfer processes from the inner Fe particles to the graphitic shells. We hypothesize that in our system the enhanced activity is accounted for by two additional factors: 1) better adsorption of O_2 on the nanotube sidewalls due to the presence of defects generated in the functionalization step, as experimentally[35] and theoretically[36] shown previously, and 2) the presence of cross-linking defects that allow better electronic communication between the internal Fe and the outer graphitic shells.[37] To support the hypothesis of better electronic communication in t-Fe@MWCNTs relative to HCl-Fe@MWCNTs, we studied the electrochemical impedance response in $K_3[Fe(CN)_6]/K_4[Fe(CN)_6]$ solution and under ORR conditions. The obtained spectra were analyzed by using the Randles and R(RC) circuits, as required. The obtained results reveal a significant decrease in the charge-transfer resistance after organic functionalization, which facilitates electron-transfer processes, in good agreement with the voltammetric results (Supporting Information, Figure S5). A deeper analysis of the ORR activity was performed by measuring the CVs in the presence of increasing O_2 concentrations (between 0 and 4 mg L^{-1}). Figure 7 shows the obtained CVs on t-Fe@MWCNT at $v = 0.10$ V s^{-1}.

A linear dependence between the peak currents and the concentration of O_2 was obtained in the range from 0.0 to 2.5 mg L^{-1}. The linear regression equation for this calibration curve was $\Delta i_{peak}/mA = 0.03 - 0.15 \times [O_2]/mg\,L^{-1}$ ($R^2 = 0.996$, $N = 9$). The sensitivity of each catalyst was determined from the slope of the calibration curve and corrected by the electroactive surface area determined by chronoamperometry. Table 1 summarizes the calculated values including the limit of detection (LOD) and the linear range.[38]

When the GCE surface was modified with MWCNTs a 27-fold enhancement of the sensitivity was found together with a decrease in LOD (from 1.02 to 0.06 mg L^{-1}), as reported by several authors.[39] The presence of the encapsulated Fe increases the sensitivity and enhances the LOD, and this improvement is more evident after exohedral functionalization.[40] In agreement with our mechanistic hypothesis and considering the general mechanism proposed by Yeager[41] for O_2 reduction, the increase in the response in the presence of the aryl-modified MWCNTs can once again be rationalized in terms of an enhanced number of defects.[42]

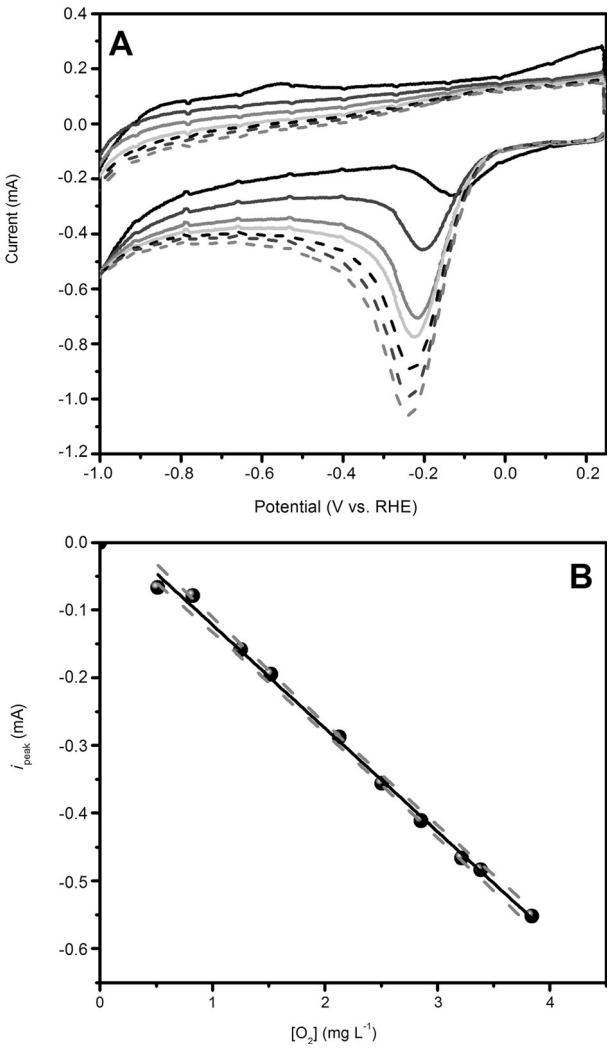

Figure 7. A) CVs at t-Fe@MWCNT-modified GCE in phosphate-buffer solution with increasing amounts of dissolved O_2. Scan rate: 0.10 V s^{-1}. B) Calibration curve obtained from the results in A). Experimental points (●), best linear fit (solid line) and 99% confidence bands (dashed line).

To investigate further the electrocatalytic performance of the above catalysts during the ORR process, linear sweep voltam-

Table 1. Figure of merits calculated for each electrode.

Structure	LOD [mg L^{-1}]	Linear range [mg L^{-1}]	Sensitivity [10^2 μA L mg^{-1} cm^{-2}][a]
GCE	1.02	3.0–4.1	0.11 ± 0.01
MWCNTs	0.06	0.2–4.0	3 ± 1
HCl-Fe@MWCNTs	0.03	0.09–2.50	4.6 ± 0.6
t-Fe@MWCNTs	0.03	0.1–3.1	8.1 ± 0.9

[a] Calculated at $E = -0.48$ V.

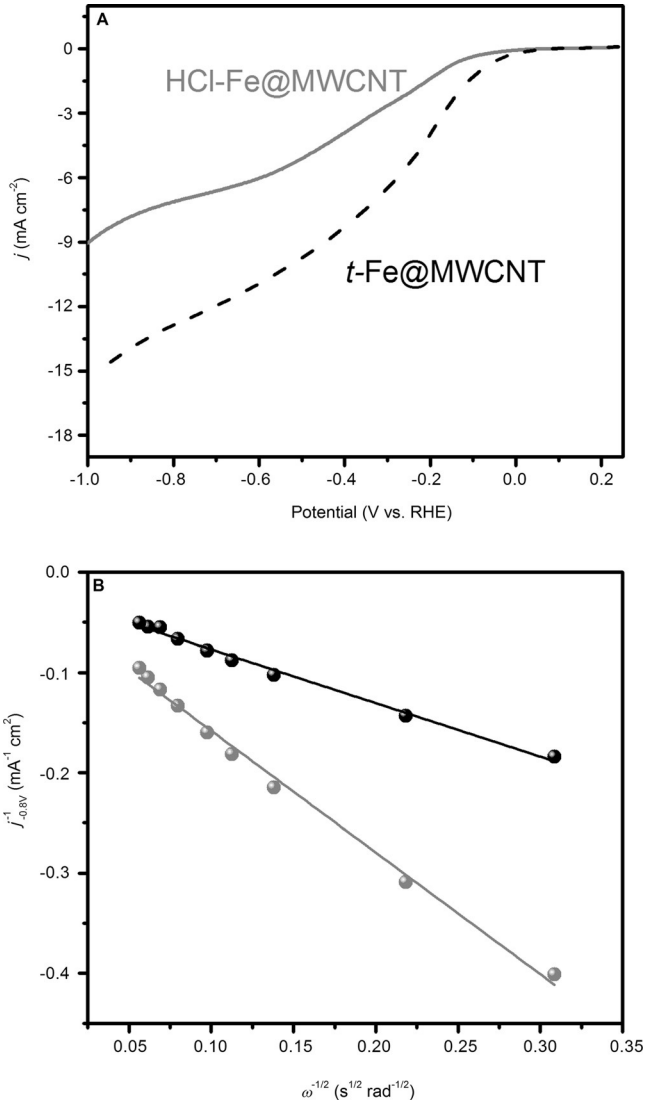

Figure 8. A) LSV curves of HCl-Fe@MWCNT- and t-Fe@MWCNT-modified GCE in O_2-saturated 0.10 M phosphate buffer solution (pH 7.40) at 1500 rpm. Scan rate: 5 mV s^{-1}. B) Corresponding K–L plots at −0.8 V versus RHE. The dots represent the experimental points and the lines the best linear fits.

metry (LSV) curves were measured with a rotating-disc electrode (RDE) at a rotation rate of 1500 rpm in O_2-saturated 0.10 M phosphate buffer solution at pH 7.40. As shown in Figure 8, t-Fe@MWCNT had a more positive onset potential (0.02 V) and higher limiting current density (−10.97 mA cm^{-2}) than HCl-Fe@MWCNTs (−0.11 V, −6.08 mA cm^{-2}), both determined at −0.8 V. These results are in perfect agreement with those obtained from CV measurements and confirm the superior catalytic activity of t-Fe@MWCNTs for the ORR. This superior activity can be related to the higher density of states on the carbon surface and the presence of cross-linking defects, which allow better electronic communication between the internal Fe and the outer graphitic shell, as we proposed previously.

The electron-transfer number *n* involved in the ORR at each electrode was analyzed by RDE and calculated on the basis of the Koutecky–Levich (K–L) Equation (1)

$$\frac{1}{j} = \frac{1}{j_K} + \frac{1.61}{nFD_{O_2}^{2/3}\nu^{-1/6}C_{O_2}\omega^{1/2}} \quad (1)$$

in which j is the measured current density, j_K the kinetic-limiting current density, n the number of electrons transferred per oxygen molecule, F the Faraday constant, D_{O_2} the diffusion coefficient of O_2 in 0.10 M phosphate buffer (2×10^{-5} cm^2 s^{-1}),[43] ν the kinetic viscosity (0.01 cm^2 s^{-1}) and C_{O_2} the bulk concentration of O_2 (0.26×10^{-3} M).[44]

The corresponding K–L plots at −0.8 V for each catalytic material (Figure 8B) are linear and thus suggest first-order dependence kinetics of the ORR.[45] According to Equation (1), *n* was estimated to be around 2 for HCl-Fe@MWCNTs and around 4 for t-Fe@MWCNTs at −0.8 V. These results indicate that, at this potential, the catalytic mechanism involving HCl-Fe@MWCNT follows a two-electron pathway, and that involving t-Fe@MWCNT a four-electron pathway.

Further insight into the ORR activity of the t-Fe@MWCNT catalyst was gained by studying the kinetics of its electrochemical response by RDE voltammetry. The polarization curves were obtained in O_2-saturated phosphate buffer solution by scanning the potential from 0.25 to −1.00 V at scan rate of 5 mV s^{-1} and rotation rates from 100 to 3000 rpm (Figure 9A). An increase in limiting current with increasing rotation rate was observed. From these results, the corresponding K–L plots were drawn (Figure 9B) and the number of electrons transferred was calculated (inset to Figure 9B). On the one hand, the extrapolated K–L lines showed non-zero intercepts indicating that the O_2 reduction process is under mixed kinetic–diffusion control. On other hand, the number of electrons gradually increased to $n=4$ with decreasing potential, which suggests that the reaction on the catalyst follows a four-electron pathway at higher applied cathodic potential. Values of *n* greater than 4 certainly result from the simultaneous reduction of water starting at potential close to −0.9 V.[44]

Hydrogen evolution reaction

To analyse the performance of t-Fe@MWCNT modified GC electrodes for HER, LSV curves were measured in N_2-saturated 0.10 M phosphate buffer solution (pH 7.40) at 0.05 V s^{-1} and room temperature (Figure 10 A). The bare GC electrode showed a large overpotential η, indicating relatively low catalytic activity of this material for the HER. A significant improvement in the catalytic performance, such as a lower onset potential and an increase in current density, was observed, in ascending order, on the MWCNT-, HCl-Fe@MWCNT- and t-Fe@MWCNT-modified electrodes. The potential at which the current increased to 0.20 mA from the baseline current was used as criterion to determine the overpotential for H_2O reduction η_c.[46] The calculated values are shown in Figure 10B.

Simply immobilizing MWCNTs on the surface of the GCE decreases the required overpotential (1.2 V). This behaviour can be explained by considering the higher hydrophilicity of the t-Fe@MWCNT-based electrodes, which improves the exohedral adsorption of H_2O and lowers the activation barrier for the re-

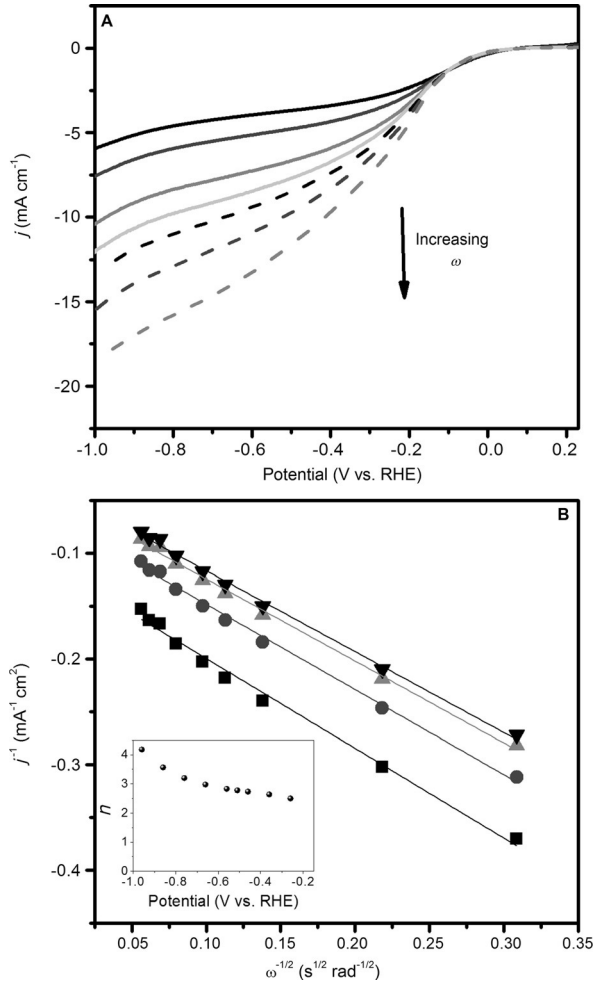

Figure 9. A) RDE curves of GCE/t-Fe@MWCNT in O_2-saturated 0.10 M phosphate buffer solution. Scan rate: 0.05 V s^{-1}. B) Correponding K–L plots at different potentials derived from the RDE measurements. Inset: *n* versus applied potential. ■ = −0.25 V; ● = −0.35 V; ▲ = −0.45 V; and ▼ = −0.50 V.

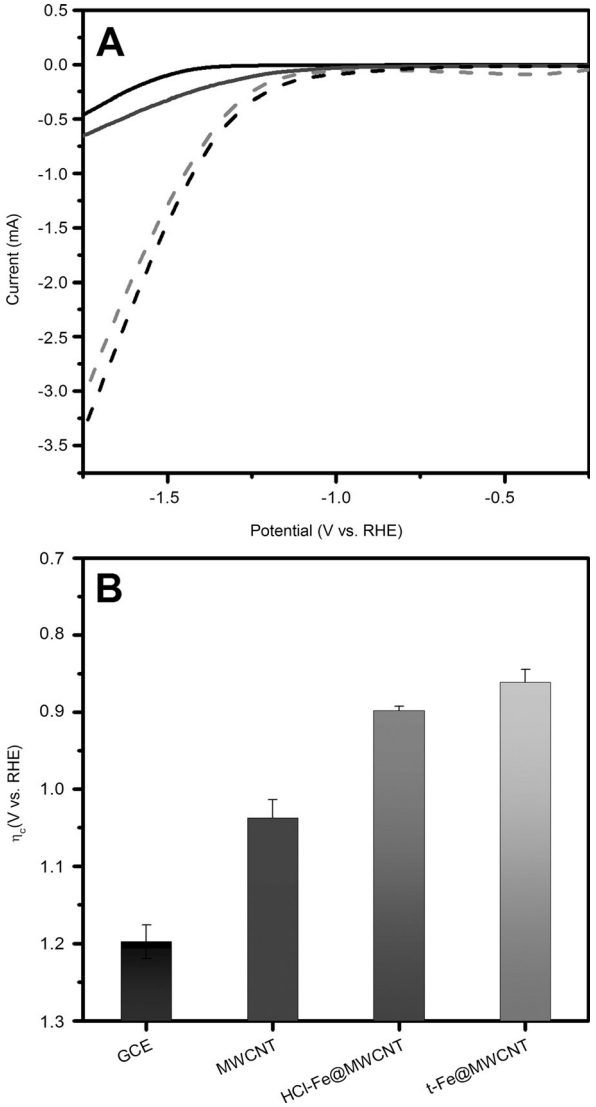

Figure 10. A) LSV of GCE (solid black), GCE/MWCNTs (solid grey), GCE/HCl-Fe@MWCNT (grey dashed), and GCE/t-Fe@MWCNT (black dashed) for HER in N_2-saturated 0.10 M phosphate buffer solution (pH 7.40). Scan rate: 0.05 V s^{-1}. B) Overpotential necessary for the hydrogen evolution reaction for the different structures.

duction reaction.[47] The presence of Fe considerably decreases the overpotential for the HER, shifting it 0.15 V to lower energy. The incorporation of the aryl moieties improves the response of the HER, reducing the overpotential by 0.05 V compared with that of HCl-Fe@MWCNT. It is well known that the electron-transport properties can play an important role in charge-transfer processes.[48] Hence, the observed improvement can be explained as a synergistic effect between the number of active reaction sites for the absorption and dissociation of H_2O and the enhanced electronic coupling between the Fe phases and the graphitic CNT walls.

Conclusion

Today, Pt-based electrodes are the common choice for many electrocatalytic energy processes, although the scarcity of Pt is an irremediable drawback for large-scale technologies. In view of the ever-growing demand for higher sustainability, we designed a functional nanocatalyst that exploits the synergy between MWCNTs and an abundant and electroactive metal (Fe). We interfaced the two components by encapsulation of Fe in the inner cavities of the MWCNTs and performed further modification by external attachment of BnCOOH groups. This material was used to assemble a working electrode, superior activity of which was demonstrated for the fuel-cell-relevant ORR (E_{onset}: 0.02 V; sensitivity: 8.9×10^2 μA L mg^{-1} cm^{-2}) and HRR (overpotential: $\eta_c = 0.8$ V) under physiological conditions. In our view, the Fe phase behaves as the true catalytic species and the MWCNTs have the double role of efficiently mediating the electron transfer to the reactive species and providing excellent protection against uncontrolled Fe oxidation or leaching. In this respect, organic functionalization can further promote electron transfer from the Fe to the external CNT layers by defect-induced electron hopping through the layers. Moreover, the organic groups favour adsorption of the reactive O_2

or H_2O molecules onto the CNT sidewalls. Our findings provide a viable alternative for using hybrid materials for fuel cells with a particular view to their favourable economics.

Experimental Section

Synthesis of Fe@MWCNT and HCl-Fe@MWCNT

In the 180 cm-long quartz tube of a furnace setup, a 10 cm long quartz substrate was introduced in the temperature region around 1173 K, and a constant flow of 0.2 $m^3 h^{-1}$ of argon was used to purge the system of remaining air. Under this flux, ferrocene (5 g) was introduced in a boat and placed in a region close to 823 K. Toluene vapour was then introduced into the quartz tube of the furnace by the argon purge of 0.2 $m^3 h^{-1}$ for 15 min. The toluene flow was then turned off and the quartz substrate was moved to a cool zone of the 180 cm long quartz tube to allow the sample to cool to room temperature under an argon flux of 0.2 $m^3 h^{-1}$. The black material was then washed with ethanol to remove any residual ferrocene to give pristine Fe@MWCNT (about 2.3 g). The material was then washed with HCl to remove any external Fe or Fe oxide (HCl-Fe@MWCNT). In detail, the as-produced material (250 mg) was placed in a 1 L round-bottomed flask, and methanol (375 mL) was added. The solution was sonicated for 10 min and a 4 M aqueous solution of hydrochloric acid (125 mL) was added to the flask. The mixture was sonicated for a further 10 min and the solution was stirred for 24 h at room temperature. The solution was diluted with water (375 mL) and then filtered through a 0.45 μm hydrophobic polytetrafluoroethylene filter. The resulting precipitate was then redispersed by 10 min of sonication in methanol (100 mL), filtered through the same filter, and washed with water (100 mL). This procedure was repeated twice, and the final precipitate was finally washed with few millilitres of methanol to facilitate drying. HCl-Fe@MWCNT was thus recovered as a black powder (about 220 mg).

Synthesis of t-Fe@MWCNT

HCl-Fe@MWCNTs (100 mg) were placed in a 500 mL round-bottomed flask and *N*-methyl-2-pyrrolidone (NMP, 67 mL) was added. The solution was sonicated for 20 min, *p*-aminophenylacetic acid (675 mg) was added, the solution was sonicated for another 10 min and diisopropylethylamine (40 μL) was added. After 10 min of further sonication, isoamyl nitrite (1.5 mL) was added slowly and the reaction mixture was stirred at 363 K for 20 h. The solution was cooled to room temperature and was filtered through a 0.45 μm hydrophobic polytetrafluoroethylene filter. The precipitate was redispersed by 10 min of sonication in 100 mL of ethyl acetate and filtered through the same filter. This step was repeated two additional times and the final precipitate was dispersed in 100 mL of methanol by 10 min of sonication, water (200 mL) was added and the suspension was filtered through the same filter. Two additional washing steps with water (50 mL) were performed. The precipitate was finally washed with few millilitres of methanol to facilitate drying. About 85 mg of t-Fe@MWCNT was thus recovered as a black powder.

Working-electrode assembly

The working electrode consisted of a GCE (Model 101, CH Instruments, ∅ 3 mm) that, prior to surface modification, was cleaned by polishing with 1.0 and 0.3 μm alumina slurries (micropolish Buehler) for 2 min and then washed with Milli-Q water. The pristine and modified MWCNTs were dispersed in a concentration of 3 mg mL^{-1} in a 1:0.09:0.02 H_2O:EtOH:Nafion (2.5 vol% in EtOH) solution by sonication for 1.5 h. Subsequently, the dispersions were centrifuged at 500 rpm for 6 min to remove residual bundles remaining in solution. CNTs were immobilized by treating the GCE with one drop of 30 μL of the CNTs dispersion and drying it for 30 min at 323 K. The resulting electrodes are denoted GCE/MWCNT, GCE/HCl-Fe@MWCNT and GCE/t-Fe@MWCNT respectively.

Physical characterization

TGA of approximately 1 mg of each compound was performed on a TGA Q500 (TA Instruments) under N_2 or under air by equilibration at 100 °C and subsequent ramp of 10 K min^{-1} up to 1073 K. Raman spectra were recorded with a Renishaw inVia microspectrometer equipped with an He–Ne laser operating at 532 nm. Powders were dispersed in ethanol, drop-cast onto a quartz slide and the solvent evaporated. At least five spectra per sample were recorded in order to check the uniformity of the materials. TEM images were acquired on a TECNAI 10 TEM. Samples were obtained by drop-casting of a 0.1 mg mL^{-1} solution of the different Fe-filled MWCNT in dichloromethane. ^{57}Fe Mössbauer spectra were recorded in transmission geometry with a Wissel GmbH spectrometer equipped with a ^{57}Co(Rh) radioactive source from Cyclotron Co operating at room temperature in the range -8 to $+8$ mm s^{-1} and calibrated with α-Fe. The spectra were fitted to a sum of Lorentzians by least-squares refinement with Recoil 1.05 Mössbauer Analysis Software.[27]

Electrochemical measurements

The electrochemical measurements were carried out at room temperature by using an Autolab potentiostat/galvanostat (Model 302N) and a RDE (Autolab), both equipped with a three-electrode cell under a stream of purified gasses that, depending on the experiment, was pure N_2 or an N_2/O_2 mixture. All potentials were measured with respect to Hg/Hg_2Cl_2, NaCl-saturated electrode (SCE) contained in a glass tube filled with the supporting electrolyte solution, separated from the solution by a Vycor frit and located close to the tip of the working electrode to minimize the ohmic drop. The counter electrode was a Pt ring directly dipped in the solution. The supporting electrolyte was composed of 0.10 M phosphate buffer solution (pH 7.40). All presented results are averages for three measurements.

Acknowledgements

The research leading to these results has received funding from the Seventh Framework Programme (FP7/2007-2013) under grant agreement n° 310651 (SACS project). M.V.B. undertook this work with the support of the "ICTP TRIL Programme, Trieste, Italy". D.B. also would like to thank the FRS-FNRS (FRFC contracts n° 2.4.550.09), the Belgian Government (IAP-PAI P7 network "Functional Supramolecular Systems") and the MIUR through the FIRB Futuro in Ricerca "SUPRACARBON'' (contract n° RBFR10DAK6). We also kindly acknowledge CONICET for the fellowship. Dr. Riccardo Marega and Florent Pineux are also acknowledged for the support in the preparation and characterization of the Fe@MWCNTs. M.V.B. thanks Dr. Foá Torres for useful comments.

Keywords: electrochemistry · iron · hydrogen evolution reaction · nanotubes · oxygen reduction reaction

[1] a) D. S. Su, G. Sun, *Angew. Chem. Int. Ed.* **2011**, *50*, 11570 – 11572; *Angew. Chem.* **2011**, *123*, 11774 – 11777; b) D. W. Wang, D. Su, *Energy Environ. Sci.* **2014**, *7*, 576 – 591; c) G. Wu, K. L. More, C. M. Johnston, P. Zelenay, *Science* **2011**, *332*, 443 – 447.

[2] A. Bielanski, J. Haber, *Chemical Industries, Vol. 43: Oxygen in Catalysis*; Marcel Dekker, New York, **1991**, p. 472.

[3] J. Wu, H. Yang, *Acc. Chem. Res.* **2013**, *46*, 1848 – 1857.

[4] F. Jaouen, E. Proietti, M. Lefevre, R. Chenitz, J. P. Dodelet, G. Wu, H. T. Chung, C. M. Johnston, P. Zelenay, *Energy Environ. Sci.* **2011**, *4*, 114 – 130.

[5] a) M. Winter, R. J. Brodd, *Chem. Rev.* **2004**, *104*, 4245 – 4269; b) S. C. Thomas, X. Ren, S. Gottesfeld, P. Zelenay, *Electrochim. Acta* **2002**, *47*, 3741 – 3748.

[6] Y. Zhu, B. Zhang, X. Liu, D. W. Wang, D. S. Su, *Angew. Chem.* **2014**, *53*, 10673 – 10677.

[7] V. I. Birss, A. Damjanovic, *J. Electrochem. Soc.* **1987**, *134*, 113 – 117.

[8] D. V. Esposito, S. T. Hunt, Y. C. Kimmel, J. G. Chen, *J. Am. Chem. Soc.* **2012**, *134*, 3025 – 3033.

[9] T. Reier, M. Oezaslan, P. Strasser, *ACS Catal.* **2012**, *2*, 1765 – 1772.

[10] a) M. W. Louie, A. T. Bell, *J. Am. Chem. Soc.* **2013**, *135*, 12329 – 12337; b) R. D. L. Smith, M. S. Prevot, R. D. Fagan, S. Trudel, C. P. Berlinguette, *J. Am. Chem. Soc.* **2013**, *135*, 11580 – 11586.

[11] M. S. Faber, S. Jin, *Energy Environ. Sci.* **2014**, *7*, 3519 – 3542.

[12] a) P. Singh, S. Campidelli, S. Giordani, D. Bonifazi, A. Bianco, M. Prato, *Chem. Soc. Rev.* **2009**, *38*, 2214 – 2230; b) D. Tasis, N. Tagmatarchis, A. Bianco, M. Prato, *Chem. Rev.* **2006**, *106*, 1105 – 1136.

[13] C. N. R. Rao, B. C. Satishkumar, A. Govindaraj, M. Nath, *ChemPhysChem* **2001**, *2*, 78 – 105.

[14] a) L. Dai, D. W. Chang, J. B. Baek, W. Lu, *Small* **2012**, *8*, 1130 – 1166; b) S. Cataldo, P. Salice, E. Menna, B. Pignataro, *Energy Environ. Sci.* **2012**, *5*, 5919 – 5940; c) A. J. Ferguson, J. L. Blackburn, N. Kopidakis, *Mater. Lett.* **2013**, *90*, 115 – 125.

[15] a) Z. Liu, L. Jiao, Y. Yao, X. Xian, J. Zhang, *Adv. Mater.* **2010**, *22*, 2285 – 2310; b) P. Avouris, *Phys. Today* **2009**, *62*, 34 – 40; c) A. M. Rawlett, H. T. Hopson, I. Amlani, R. Zhang, J. Tresek, L. A. Nagahara, R. K. Tsui, H. Goronkin, *Nanotechnology* **2003**, *14*, 377 – 384.

[16] a) Z. Chen, X. Zhang, R. Yang, Z. Zhu, Y. Chen, W. Tan, *Nanoscale* **2011**, *3*, 1949 – 1956; b) C. Fabbro, H. Ali-Boucetta, T. Da Ros, K. Kostarelos, A. Bianco, M. Prato, *Chem. Commun.* **2012**, *48*, 3911 – 3926; c) E. N. Primo, F. A. Gutierrez, G. L. Luque, P. R. Dalmasso, A. Gasnier, Y. Jalit, M. Moreno, M. V. Bracamonte, M. E. Rubio, M. L. Pedano, M. C. Rodriguez, N. F. Ferreyra, M. D. Rubianes, S. Bollo, G. A. Rivas, *Anal. Chim. Acta* **2013**, *805*, 19 – 35.

[17] a) M. Melchionna, M. Bonchio, F. Paolucci, M. Prato, P. Fornasiero, *Top Curr. Chem.* **2014**, *348*, 139 – 180; b) B. Wu, Y. Kuang, X. Zhang, J. Chen, *Nano Today* **2011**, *6*, 75 – 90; c) M. Cargnello, M. Grzelczak, B. Rodriguez-Gonzalez, Z. Syrgiannis, K. Bakhmutsky, V. La Parola, L. Liz-Marzan, R. J. Gorte, M. Prato, P. Fornasiero, *J. Am. Chem. Soc.* **2012**, *134*, 11760 – 11766.

[18] a) A. N. Khlobystov, *ACS Nano* **2011**, *5*, 9306 – 9312; b) D. A. Britz, A. N. Khlobystov, *Chem. Soc. Rev.* **2006**, *35*, 637 – 659; c) R. Marega, D. Bonifazi, *New J. Chem.* **2014**, *38*, 22 – 27.

[19] E. G. Derouane, *J. Mol. Catal. A* **1998**, *134*, 29 – 45.

[20] J. P. Tessonnier, O. Ersen, G. Weinberg, C. Pham-Huu, D. S. Su, R. Schlogl, *ACS Nano* **2009**, *3*, 2081 – 2089.

[21] D. Deng, L. Yu, X. Chen, G. Wang, L. Jin, X. Pan, J. Deng, G. Sun, X. Bao, *Angew. Chem.* **2013**, *52*, 371 – 375.

[22] a) L. Feng, Y. Yan, Y. Chen, L. Wang, *Energy Environ. Sci.* **2011**, *4*, 1892 – 1899; b) S. Li, Y. Hu, Q. Xu, J. Sun, B. Hou, Y. Zhang, *J. Power Sources* **2012**, *213*, 265 – 269.

[23] F. Scholz, U. Schroeder, S. Meyer, K. Z. Brainina, N. F. Zakharchuk, N. V. Sobolev, O. A. Kozmenko, *J. Electroanal. Chem.* **1995**, *385*, 139 – 142.

[24] a) B. E. Logan, J. M. Regan, *Environ. Sci. Technol.* **2006**, *40*, 5172 – 5180; b) B. E. Logan, B. Hamelers, R. Rozendal, U. Schroeder, J. Keller, S. Freguia, P. Aelterman, W. Verstraete, K. Rabaey, *Environ. Sci. Technol.* **2006**, *40*, 5181 – 5192; c) C. Picioreanu, I. M. Head, K. P. Katuri, M. C. M. van Loosdrecht, K. Scott, *Water Res.* **2007**, *41*, 2921 – 2940.

[25] a) X. Zou, X. Huang, A. Goswami, R. Silva, B. R. Sathe, E. Mikmeková, T. Asefa, *Angew. Chem.* **2014**, *126*, 4461 – 4465; b) J. Tian, Q. Liu, A. M. Asiri, X. Sun, *J. Am. Chem. Soc.* **2014**, *136*, 7587 – 7590; c) C. Di Giovanni, W. A. Wang, S. Nowak, J. M. Grenèche, H. Lecoq, L. Mouton, M. Giraud, C. Tard, *ACS Catal.* **2014**, *4*, 681 – 687.

[26] a) M. A. Hamon, J. Chen, H. Hu, Y. Chen, M. E. Itkis, A. M. Rao, P. C. Eklund, R. C. Haddon, *Adv. Mater.* **1999**, *11*, 834 – 840; b) J. Liu, A. G. Rinzler, H. Dai, J. H. Hafner, R. K. Bradley, P. J. Boul, A. Lu, T. Iverson, K. Shelimov, C. B. Huffman, F. Rodriguez-Macias, Y. S. Shon, T. R. Lee, D. T. Colbert, R. E. Smalley, *Science* **1998**, *280*, 1253 – 1256.

[27] K. Lagarec, D. G. Rancourt, *Recoil, Mössbauer Spectral Analysis Software for Windows*, version 1.0; Department of Physics, University of Ottawa: Ottawa, Canada, **1998**.

[28] R. Marega, F. De Leo, F. Pineux, J. Sgrignani, A. Magistrato, A. D. Naik, Y. Garcia, L. Flamant, C. Michiels, D. Bonifazi, *Adv. Funct. Mater.* **2013**, *23*, 3173 – 3184.

[29] J. L. Bahr, J. M. Tour, *Chem. Mater.* **2001**, *13*, 3823 – 3824.

[30] D. Bonifazi, C. Nacci, R. Marega, S. Campidelli, G. Ceballos, S. Modesti, M. Meneghetti, M. Prato, *Nano Lett.* **2006**, *6*, 1408 – 1414.

[31] A. Dumitru, M. Mamlouk, K. Scott, *Electrochim. Acta* **2014**, *135*, 428 – 438.

[32] L. Bokobza, J. L. Bruneel, M. Couzi, *Vib. Spectrosc.* **2014**, *74*, 57 – 63.

[33] M. Hoefer, P. R. Bandaru, *Appl. Phys. Lett.* **2009**, *95*, 183108/1 – 183108/3.

[34] a) J. L. Lyon, K. L. Stevenson, *Langmuir* **2007**, *23*, 11311 – 11318; b) A. Doménech-Carbó, S. Sánchez-Ramosa, M. T. Doménech-Carbó, J. V. Gimeno-Adelantado, F. Bosch-Reig, D. J. Yusá-Marco, M. C. Aurí-París, *Electroanalysis* **2002**, *14*, 685 – 696.

[35] H. Ulbricht, G. Moos, T. Hertel, *Surf. Sci.* **2003**, *532 – 535*, 852 – 856.

[36] a) D. C. Sorescu, K. D. Jordan, P. Avouris, *J. Phys. Chem. B* **2001**, *105*, 11227 – 11232; b) X. Qi, X. Guo, C. Zheng, *Appl. Surf. Sci.* **2012**, *259*, 195 – 200.

[37] S. Agrawal, M. S. Raghuveer, H. Li, G. Ramanath, *Appl. Phys. Lett.* **2007**, *90*, 193104/1 – 193104/3.

[38] a) A. Shrivastava, V. Gupta, *Chron. Young Sci.* **2011**, *2*, 21 – 25; b) V. Gold, *Compendium of Chemical Terminology*, Blackwell Scientific Publications, Oxford, **1987**.

[39] K. Waki, R. A. Wong, H. S. Oktaviano, T. Fujio, T. Nagai, K. Kimoto, K. Yamada, *Energy Environ. Sci.* **2014**, *7*, 1950 – 1958.

[40] K. M. Samant, V. S. Joshi, K. R. Patil, S. K. Haram, *Bull. Mater. Sci.* **2014**, *37*, 221 – 226.

[41] E. J. Yeager, *Mol. Catal.* **1986**, *38*, 5 – 25.

[42] a) R. S. Zhong, Y. H. Qin, D. F. Niu, J. W. Tian, X. S. Zhang, X. G. Zhou, S. G. Sun, W. K. Yuan, *J. Power Sources* **2013**, *225*, 192 – 199; b) C. Domínguez, F. J. Perez-Alonso, M. Abdel Salam, S. A. Al-Thabaiti, A. Y. Obaid, A. A. Alshehri, J. L. Gomez de La Fuente, J. L. G.; Fierro, S. Rojas, *Appl. Catal. B* **2015**, *162*, 420 – 429; Fierro, S. Rojas, *Appl. Catal. B* **2015**, *162*, 420 – 429.

[43] R. N. Adams, *Electrochemistry at Solid Electrodes*, Marcel Dekker, New York, **1969**.

[44] G. Gotti, K. Fajerwerg, D. Evrard, P. Gros, *Int. J. Electrochem. Sci.* **2013**, *8*, 12643 – 12657.

[45] A. J. Bard, L. R. Faulkner, *Electrochemical Methods. Findamentals and Applications*, Wiley, New York, **2001**.

[46] J. Zhang, *PEM Fuel Cell Electrocatalysts and Catalyst Layers*, Springer, London, **2008**.

[47] a) Y. Cheng, C. Xu, L. Jia, J. D. Gale, L. Zhang, C. Liu, P. K. Shen, S. P. Jiang, *Appl. Catal. B* **2015**, *163*, 96 – 104; b) I. Dumitrescu, N. R. Wilson, J. V. Macpherson, *J. Phys. Chem. C* **2007**, *111*, 12944 – 12953.

[48] R. A. Marcus, *Can. J. Chem.* **1959**, *37*, 155 – 163.